

## HIGGS HIGHLIGHTS AT ATLAS

L. MIJOVIĆ, on behalf of the ATLAS collaboration  
*SUPA - School of Physics and Astronomy*  
*University of Edinburgh, United Kingdom*

As the Higgs boson turns 10 this Summer, and the Large Hadron Collider experiments eagerly await the next round of data-taking, the ATLAS collaboration has recently reached important new insights into the Higgs mechanism. This report is a snapshot of Higgs highlights for the MoriondQCD conference, obtained with  $139 \text{ fb}^{-1}$  of Run2 proton–proton collision data taken at centre-of-mass energy of 13 TeV.

### 1 Higgs Boson Production and Decay

At the Large Hadron Collider (LHC) the Higgs boson is produced through gluon-gluon fusion (ggF) 87% of the time, followed by vector boson fusion (VBF, 7%) associated weak gauge boson production ( $VH$ , 4%), associated top-antitop production ( $t\bar{t}H$ , 1%), and other production modes with small cross-sections<sup>1</sup>. The mass of the Higgs boson is measured to be  $m_H=125.09 \text{ GeV}$ <sup>2</sup>, at which the Standard Model (SM) Higgs boson decays to  $b\bar{b}$  pairs most of the time, with a branching ratio (BR) of  $\sim 58.1\%$ . However, in several measurements the highest sensitivity is achieved in final states detected with higher purity and resolution, in particular  $H \rightarrow \tau\tau$  decay with  $\text{BR} \sim 6.26\%$ ,  $H \rightarrow \gamma\gamma$  decay with  $\text{BR} \sim 0.227\%$  and  $H \rightarrow ZZ^* \rightarrow 4\ell$  ( $\ell = e, \mu$ ) decay with a branching ratio of only  $\sim 0.0125\%$ <sup>1</sup>.

### 2 Higgs Boson Cross-Section and Coupling Strength Measurements

With the Run2 data the uncertainty on the Higgs boson production cross-section and coupling measurements has reached sub-10% and sub-5% respectively. In a combination of  $H \rightarrow \gamma\gamma$  and  $H \rightarrow ZZ^* \rightarrow 4\ell$  decays ATLAS<sup>3</sup> has measured the inclusive cross-section with 7% uncertainty:

$$\sigma(pp \rightarrow H) = 55.5_{-3.8}^{+4.0} \text{ pb} = 55.5 \pm 3.2 \text{ (stat.) } {}_{-2.2}^{+2.4} \text{ (sys.) pb}, \quad (1)$$

where (stat.) and (sys.) denote the statistical and systematic uncertainty respectively<sup>4</sup>. The measured value is compatible with the SM prediction of  $55.6 \pm 2.5 \text{ pb}$ <sup>1</sup>, and the statistical uncertainty of 6% dominates over the 4% systematic uncertainty. The cross-section is also measured differentially; Figure 1 shows the cross-sections as a function of the Higgs boson's rapidity  $|y_H|$  sensitive to parton distribution functions (PDF), and the transverse momentum of the Higgs boson ( $p_T^H$ ) sensitive to perturbative QCD calculations. The measurements in the  $H \rightarrow \gamma\gamma$  and  $H \rightarrow ZZ^* \rightarrow 4\ell$  decays are compatible with a p-value of 23% for  $|y_H|$  and 20% for  $p_T^H$ . The measurements are compared to the theory predictions for the ggF production, assuming SM predictions for the production modes other than the ggF. For  $|y_H|$  the combined measurement is

compatible with all the considered predictions with p-value  $\geq 92\%$ . The predictions are obtained with PDF4LHC NNLO PDF (NNLOPS, ResBos2 and SCETlib) and NNPDF30 NLO PDF set (MG5FxFx). For  $p_T^H$  the p-values range between 3.1% (RadiSH) and 78% (NNLOPS).

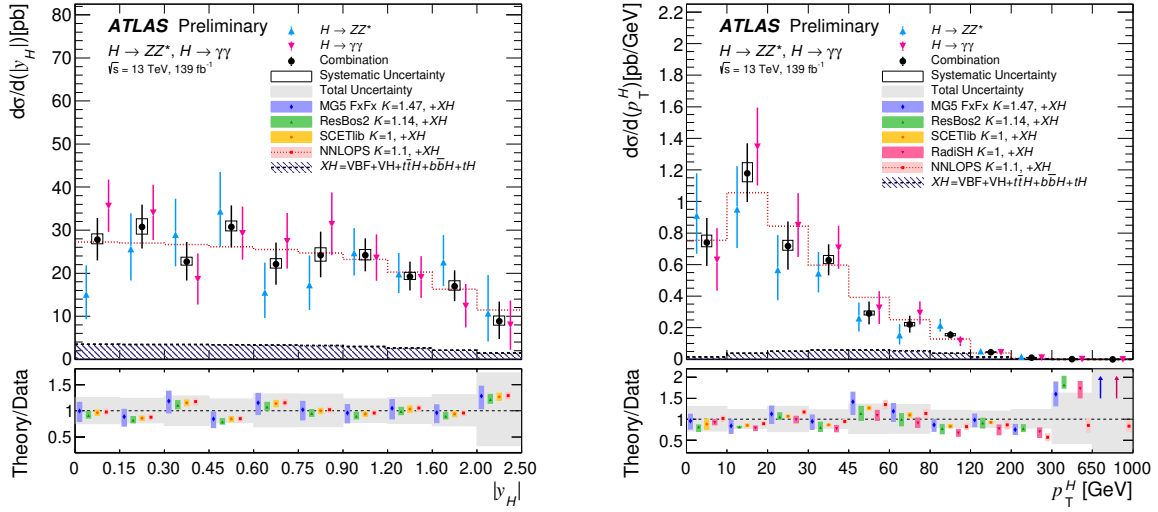


Figure 1 – Differential cross-section measurements as a function of  $|y_H|$  (left) and  $p_T^H$  (right) compared to the theory predictions for the ggF production<sup>4</sup>.

In the combination of  $H \rightarrow \gamma\gamma$ ,  $ZZ^*$ ,  $WW^*$ ,  $\tau\tau$ ,  $b\bar{b}$ ,  $\mu\mu$ ,  $Z\gamma$  decay modes and searches for decay into invisible final states<sup>5</sup>, the cross-sections for the main production modes have been measured with uncertainties of  $\lesssim 23\%$ , and the systematic uncertainty is about the same size as the statistical uncertainty, as shown in Figure 2 (left).

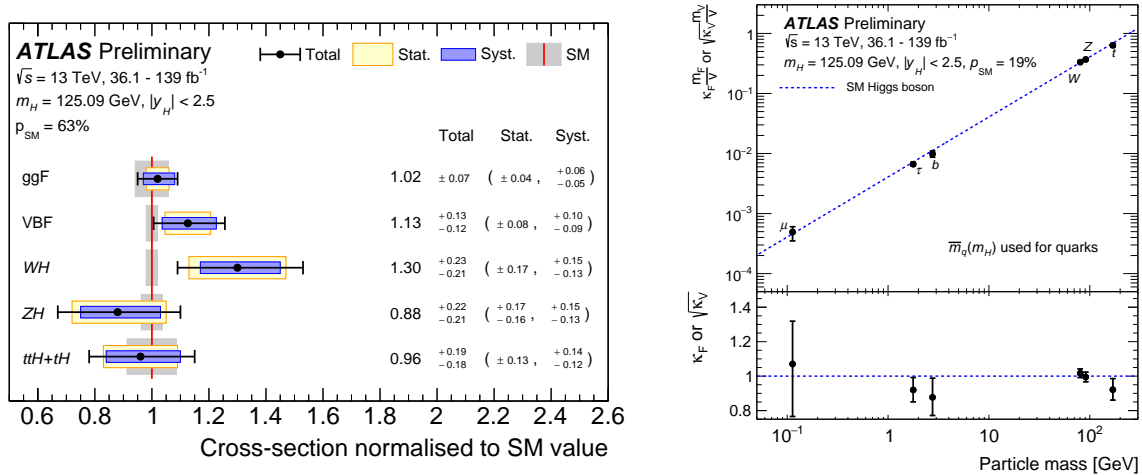


Figure 2 – Left: cross-sections for ggF, VBF, WH, ZH and  $t\bar{t}H+tH$  production modes. Right: coupling strength modifiers for fermions  $F=(t, b, \tau, \mu)$  and weak gauge bosons  $V$ . The dashed line shows the SM prediction<sup>5</sup>.

The cross-section measurements can be interpreted in terms of coupling strengths of the Higgs field to fermions or weak gauge bosons as shown in Figure 2 (right). Although these coupling strengths are compatible with the SM, there are several gaps in our experimental knowledge, due to which we can not claim to have verified that the Higgs couplings are as predicted by the SM. These include: (1) a model-independent extraction of the couplings. The couplings are obtained from cross-sections, assuming no interactions between the Higgs boson and BSM particles, and taking the width of the Higgs boson to be as predicted by the SM; (2) measurement of the 1st and 2nd generation fermion couplings; (3) measurement of the Higgs self-coupling. Efforts to address (1) include Effective Field Theory interpretations and measurements of the Higgs width. The next two sections review the large progress ATLAS has recently made on (2) and (3).

### 3 Search for $VH, H \rightarrow c\bar{c}$ Production

The search for  $H \rightarrow c\bar{c}$  decays<sup>6</sup> is performed in  $VH$  production. This is the golden production mode for measurements of  $H \rightarrow b\bar{b}$  decays, because the leptonic decay of the weak gauge boson enables efficient triggering and background rejection. In addition to challenges faced by  $H \rightarrow b\bar{b}$  measurements, the  $H \rightarrow c\bar{c}$  analysis deals with:

- low branching ratio:  $\text{BR}(H \rightarrow c\bar{c}) = 2.89\%$ , about 20 times smaller than the  $\text{BR}(H \rightarrow b\bar{b})$ .
- Charm tagging, which requires identification of charm-hadron decays with less distinct signature compared to  $B$ -hadron decays.

Separating charm-jets from  $b$ -jets is particularly challenging; this is addressed by a dedicated charm tagging algorithm, which requires the jets to have a high  $c$ -tagging score as well as vetoing jets with high  $b$ -tagging scores. This veto makes the signal events in  $H \rightarrow c\bar{c}$  and  $H \rightarrow b\bar{b}$  analyses orthogonal and enables their combination.

The  $VH, H \rightarrow c\bar{c}$  analysis extracts the signal and backgrounds from a simultaneous fit to invariant mass of the  $c$ -tagged jets ( $m_{c\bar{c}}$ ). In the fit, three signal strengths ( $\mu$ ), which multiply the SM cross-sections, are extracted:  $\mu_{VH(c\bar{c})}$ , and the di-boson production signal strengths  $\mu_{VW(cq)}$  and  $\mu_{VZ(c\bar{c})}$ . Figure 3 (left) shows the best-fit distributions (solid histograms) compared to the data. The solid line corresponds to the 95% confidence level (CL) upper limit,  $\mu_{VH(c\bar{c})} = 26$ .

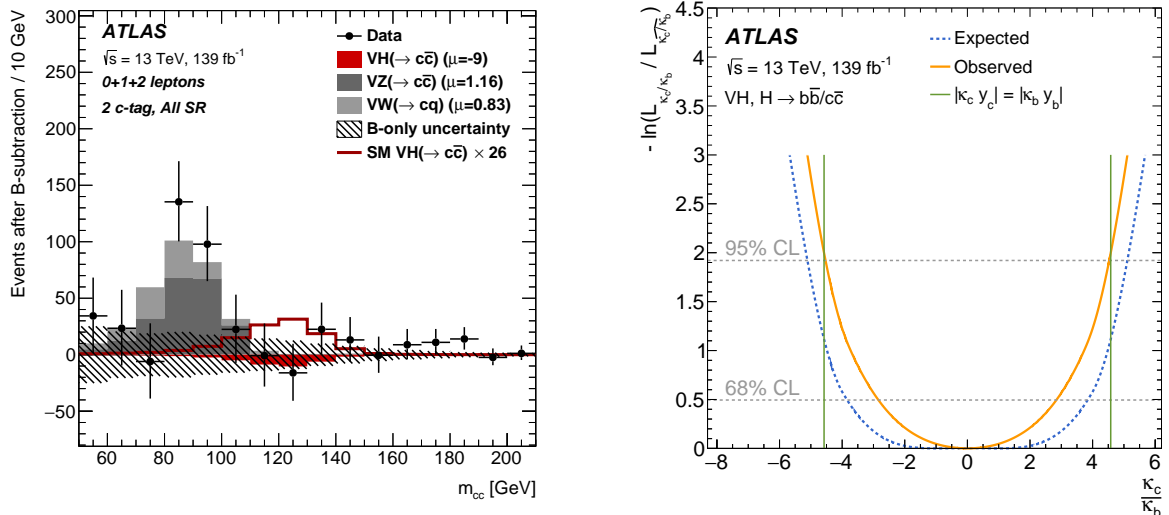


Figure 3 – Left: signal strength ( $\mu$ ) fit to  $m_{c\bar{c}}$  in the search for  $VH, H \rightarrow c\bar{c}$  events. Right: constraints on coupling modifier ratio  $|\kappa_c/\kappa_b|$  obtained in a combination of  $VH, H \rightarrow c\bar{c}$  and  $VH, H \rightarrow b\bar{b}$  analyses<sup>6</sup>.

A combination of  $H \rightarrow c\bar{c}$  and  $H \rightarrow b\bar{b}$  analyses is performed, and interpreted in terms of constraints on the ratio:  $|\kappa_c/\kappa_b|$ . The coupling strength modifiers ( $\kappa$ ) are defined as the ratios of the measured Yukawa couplings ( $y$ ) and their SM values:  $\kappa_c = y_c/y_c^{\text{SM}}$  and  $\kappa_b = y_b/y_b^{\text{SM}}$ . Within the SM  $y_b$  exceeds  $y_c$  by a factor equal to the ratios of the  $b$ - and  $c$ -quark masses:  $m_b/m_c = 4.578 \pm 0.008$ <sup>7</sup>. Figure 3 (right) shows the observed bound:  $|\kappa_c/\kappa_b| < 4.5$  at 95% CL. This is slightly smaller than the ratio  $m_b/m_c$  shown in vertical lines, which means that the Higgs-charm coupling is weaker than the Higgs-bottom coupling. This important result requires no assumptions about the width of the Higgs boson, because the bound is extracted from the ratio of the coupling modifiers rather than from their absolute values.

### 4 Searches for Di-Higgs Production

Di-Higgs production is a probe of the Higgs potential  $V$ , which can be expanded around its minimum by an excitation ( $h$ ) of the Higgs field as:

$$V(h) = \frac{1}{2}m_H h^2 + \lambda_3 v h^3 + \frac{1}{4}\lambda_4 h^4. \quad (2)$$

Within the SM the self-couplings are:  $\lambda_3^{\text{SM}} = \lambda_4^{\text{SM}} = m_H^2/(2v^2)$ . The di-Higgs searches probe the trilinear coupling  $\lambda_3$ , parameterised by the coupling modifier  $\kappa_\lambda = \lambda_3/\lambda_3^{\text{SM}}$ . At the LHC, the di-Higgs production proceeds through ggF  $\sim 95\%$  of the time. The second largest contribution is from VBF production. The corresponding diagrams are shown in Figure 4.

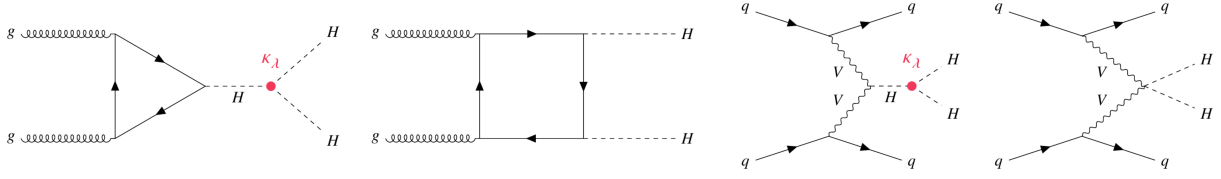


Figure 4 – The ggF and VBF di-Higgs production diagrams.

The diagrams with and without the trilinear coupling interfere destructively, leading to small cross-sections:  $\sigma_{\text{ggF}}(pp \rightarrow HH) = 31.05 \text{ fb}$  and  $\sigma_{\text{VBF}}(pp \rightarrow HH) = 1.73 \text{ fb}$ . Due to this, the highest sensitivity is achieved in searches in which one of the Higgs bosons decays to  $b\bar{b}$  pair with the highest branching ratio, shown in the first column of Figure 5 (left), and the other Higgs boson decays to a distinct signature:  $H \rightarrow \tau\tau$  or  $H \rightarrow \gamma\gamma$ . The observed and expected limits on the signal strength  $\sigma(pp \rightarrow HH)/\sigma(pp \rightarrow HH)^{\text{SM}}$  from these decay modes, and their combination, are shown in Figure 5 (right).

	bb	WW	$\tau\tau$	ZZ	$\Upsilon\Upsilon$
bb	34%				
WW	25%	4.6%			
$\tau\tau$	7.3%	2.7%	0.39%		
ZZ	3.1%	1.1%	0.33%	0.069%	
$\Upsilon\Upsilon$	0.26%	0.10%	0.028%	0.012%	0.0005%

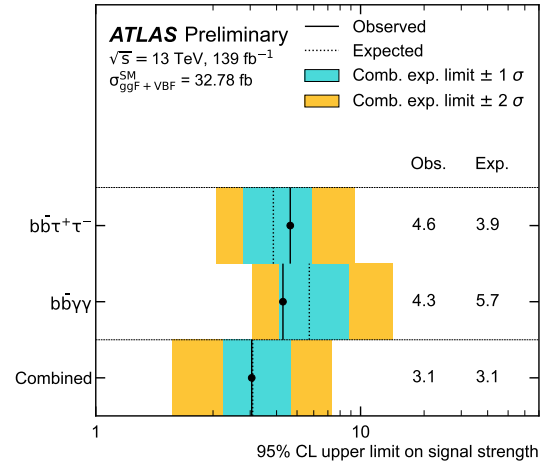


Figure 5 – Branching ratios for  $HH$  production (left) and upper limit on the  $HH$  signal strength (right)<sup>8</sup>.

The measured cross-sections can be interpreted in terms of bounds on  $\kappa_\lambda$ . The observed 95% CL bound is:  $\kappa_\lambda \in [-1.0, 6.6]$ <sup>8</sup>, as shown in Figure 6 (left).

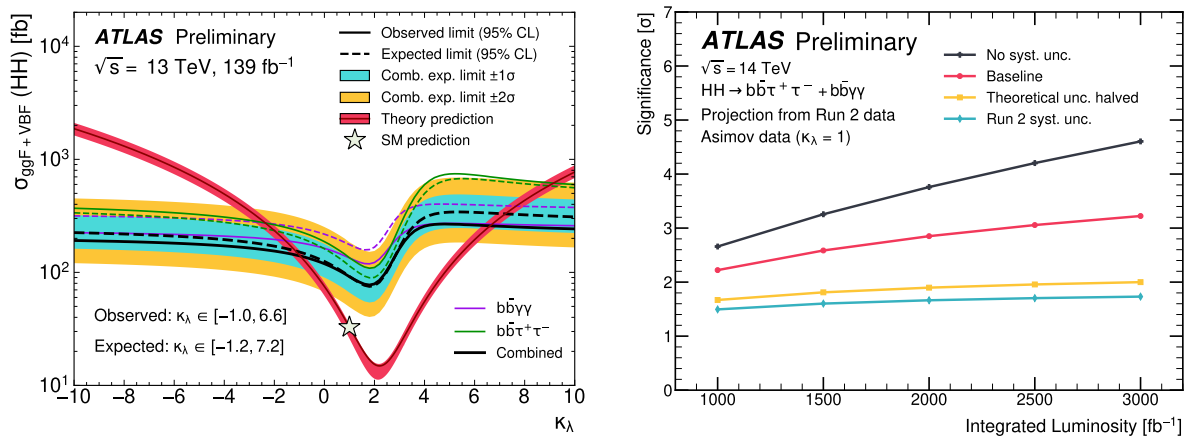


Figure 6 – Left: bounds on the di-Higgs production cross-section and trilinear coupling modifier ( $\kappa_\lambda$ ) with the Run2 data<sup>8</sup>. Right: expected significance of di-Higgs searches at the HL-LHC<sup>9</sup>.

Searches with Run2 data are limited by statistical uncertainty. To gauge the potential for di-Higgs observation, it is therefore important to extrapolate the sensitivity to the future high-luminosity LHC (HL-LHC), as shown in Figure 6 (right). If no systematic uncertainty is considered, the  $HH$  signal strength would be measured with 23% statistical uncertainty with the HL-LHC data-set of  $3000 \text{ fb}^{-1}$ . Accounting for systematic uncertainty, with a baseline estimate of how this uncertainty will evolve, the signal strength is projected to be measured with  $+34\%$   $-31\%$  uncertainty, constraining trilinear coupling modifier to  $\kappa_\lambda \subset [0.5, 1.6]$  at  $1 \sigma$  CL <sup>9</sup>.

## 5 New Results for MoriondQCD

ATLAS results made available for the first time for the MoriondQCD conference include: a new probe of the charge conjugation and parity (CP) of the top-Higgs coupling <sup>10</sup>, and a measurement of the fiducial and differential cross-section of  $VH$  production <sup>11</sup>.

The SM predicts the top-quark Yukawa coupling ( $y_t$ ) to be CP-even, however a presence of a CP-odd admixture has not yet been excluded. With a CP mixing angle  $\alpha$  the contribution to the Lagrangian is parameterised as:

$$\mathcal{L} = -y_t \bar{\Psi}_t \kappa'_t (\cos(\alpha) + i \sin(\alpha) \gamma^5) \Psi_t \Phi. \quad (3)$$

The new analysis extracts  $\alpha$  and the coupling strength modifier  $\kappa'_t$  and targets the final states with top quarks and  $H \rightarrow b\bar{b}$  decays. The main challenge is constraining non-resonant  $t\bar{t} + b\bar{b}$  background, which dominates the measurement uncertainty. The angle  $\alpha$  is extracted from fits to CP-sensitive observables, such as:

$$b_4 = \frac{p_t^z p_{\bar{t}}^z}{|\vec{p}_t| |\vec{p}_{\bar{t}}|}, \quad (4)$$

where  $p^z$  and  $\vec{p}$  are the longitudinal momentum and the momentum three-vector of the top and anti-top quark candidates. Figure 7 (left) shows the distribution of the variable  $b_4$  for CP-even ( $\alpha = 0^\circ$ ) and pure CP-odd ( $\alpha = 90^\circ$ ) hypotheses. In the CP-odd case, the top and anti-top are more likely to fly in the opposite directions, therefore  $b_4$  is more likely to be negative. The data disfavors the pure CP-odd coupling at  $1.2 \sigma$  significance. The best-fit value, shown in Figure 7 (right), is:  $\alpha = 11^\circ \text{ }^{+56^\circ}_{-77^\circ}$ . This is consistent with the previously published ATLAS measurement of the CP-properties of the top-Higgs coupling in  $H \rightarrow \gamma\gamma$  decays, which sets a constraint:  $|\alpha| < 43^\circ$  at 95% CL and excludes pure CP-odd coupling at  $3.9 \sigma$  significance <sup>12</sup>.

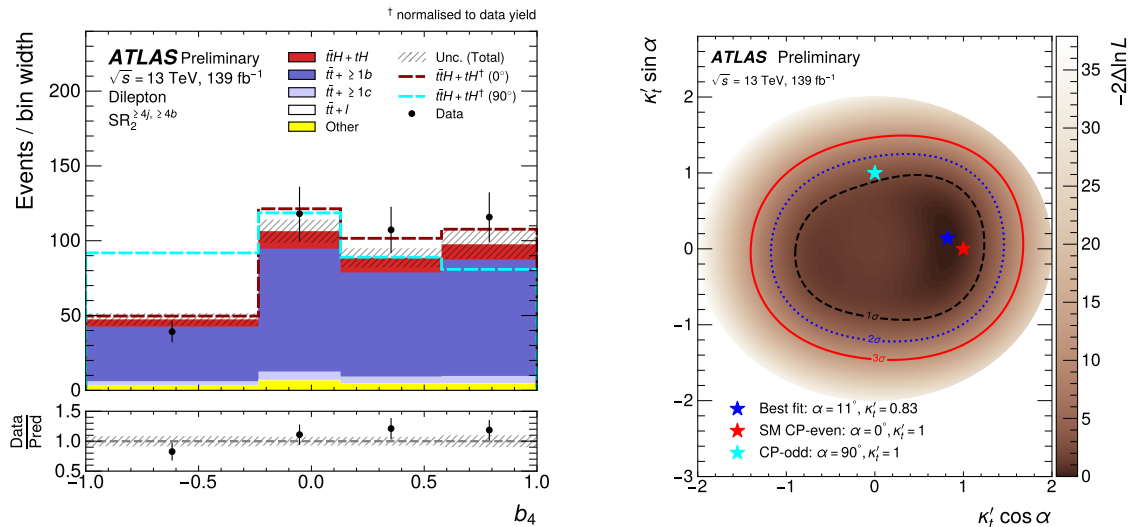


Figure 7 – Left: fit to observable  $b_4$ , used to constrain the CP properties of the top-Higgs coupling. Right: the observed constraints on the coupling modifier ( $\kappa'_t$ ) and the CP mixing angle ( $\alpha$ ) <sup>10</sup>.

The new fiducial and differential cross-section measurement of the  $VH$  production targets  $H \rightarrow b\bar{b}, Z \rightarrow \nu\nu$  decays. The idea behind the *fiducial* measurements is to use particle-level selection criteria close to the detector acceptance. Such measurements require no extrapolation outside the measured phase-space, which minimises model dependence. The new measurement extracts the signal strengths from a fit to the invariant mass  $m_{b\bar{b}}$ , shown in Figure 8 (left). The neutrinos are reconstructed as missing transverse energy  $E_T^{\text{miss}}$ , and the signal strengths are extracted in two bins:  $150 \text{ GeV} < E_T^{\text{miss}} < 250 \text{ GeV}$  and  $E_T^{\text{miss}} > 250 \text{ GeV}$ , as shown in Figure 8 (right).

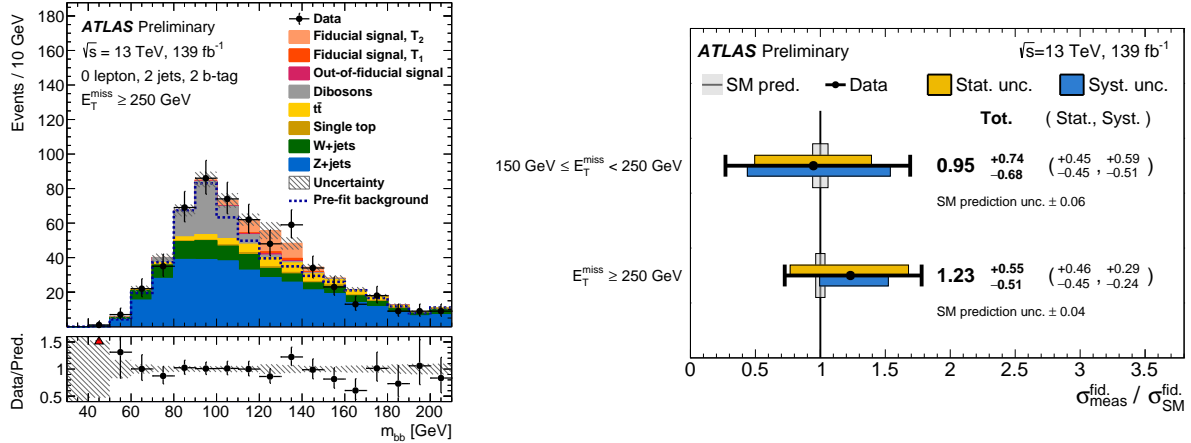


Figure 8 – Left: invariant mass spectrum fit, used to measure  $VH, H \rightarrow b\bar{b}$  fiducial cross-sections. The T1 and T2 denote two  $E_T^{\text{miss}}$  bins:  $150 \text{ GeV} < E_T^{\text{miss}} < 250 \text{ GeV}$  and  $E_T^{\text{miss}} > 250 \text{ GeV}$ . Right: the measured signal strengths<sup>11</sup>.

The new fiducial measurement is complementary to previously published ATLAS  $VH, H \rightarrow b\bar{b}$  results, which measure the cross-section extrapolated to simplified volumes in so-called *Simplified Template Cross-Section* (STXS) framework<sup>13</sup>. These measure the  $WH$  and  $ZH$  production cross-sections with  $4.0\sigma$  and  $5.3\sigma$  significance respectively.

## 6 Summary

Within a decade of the Higgs boson discovery, ATLAS has observed all main production modes and measured the inclusive production cross-section with 7% uncertainty. The quest for new experimental probes of the Higgs mechanism continues and measurements with the LHC Run2 data have advanced our knowledge. New break-throughs in answering the major open questions are: (1) a measurement confirming that the charm-quark Yukawa coupling is smaller than the  $b$ -quark coupling; (2) enhanced sensitivity of di-Higgs production searches, with an extrapolated di-Higgs cross-section measurement sensitivity of  $^{+34\%}_{-31\%}$  at the HL-LHC.

## References

1. D. de Florian et al., [arXiv:1610.07922](#) (2017).
2. ATLAS and CMS Collaborations, *Phys. Rev. Lett.* **114**, 191803 (2015).
3. ATLAS Collaboration, *JINST* **3**, S08003 (2008).
4. ATLAS Collaboration, [ATLAS-CONF-2022-002](#) (2022).
5. ATLAS Collaboration, [ATLAS-CONF-2021-053](#) (2021).
6. ATLAS Collaboration, [arXiv:2201.11428](#) (2022).
7. A. Bazavov et al., *Phys. Rev. D* **98**, 054517 (2018).
8. ATLAS Collaboration, [ATLAS-CONF-2021-052](#) (2021).
9. ATLAS Collaboration, [ATL-PHYS-PUB-2022-005](#) (2022).
10. ATLAS Collaboration, [ATLAS-CONF-2022-016](#) (2022).
11. ATLAS Collaboration, [ATLAS-CONF-2022-015](#) (2022).
12. ATLAS Collaboration, *Phys. Rev. Lett.* **125**, 061802 (2020).
13. ATLAS Collaboration, *Eur. Phys. J. C* **81**, 178 (2021).